www.arpnjournals.com

METAL DUSTING BEHAVIOUR OF FURNACE TUBE ALLOYS

Abdulaziz Al-Meshari[1] and John Little[2]
[1]SABIC Technology Centre-Jubail, Jubail Industrial City, Saudi Arabia
[2]Department of Materials Science and Metallurgy, University of Cambridge, Cambridge, UK
E-Mail: meshariai@sabic.com

ABSTRACT

Metal dusting has long been a chronic problem for several industrial sectors. In order to obtain a better understanding of the aspects of this failure mode, three heat-resistant alloys, KHR35C HiSi©, KHR45A LC©, and UCX© were exposed to a gas mixture of 80 vol% CO+20 vol% H_2 flowing at $100cm^3$ min^{-1} at 650, 750, and 850ºC for 100h. The alloys were then characterized by visual examination, XRD, and SEM/EDX. In conclusion, KHR35C HiSi© suffered localized metal dusting at 650 and 750ºC and the attack became less aggressive with the temperature increase. The least attack on KHR35C HiSi© was however observed after exposure at 850ºC. The corrosion mode at each temperature was also elucidated. Pitting also occurred on KHR45A LC© after exposure at 650ºC but to a lesser degree compared to KHR35C HiSi©. Moreover, a few pits were observed on KHR45A LC© exposed at 750ºC with the least took place at 850ºC. UCX©, which contained the highest concentrations of chromium and nickel, exhibited the best resistance to metal dusting at the test temperatures.

Keywords: metal dusting, carburisation, oxidation, heat-resistant alloys.

INTRODUCTION

Engineering alloys are vulnerable to metal dusting when exposed to strongly carburising environments at elevated temperatures, whereby the alloys corrode to produce metal, metal carbide, carbon, and oxide particles. The temperatures at which metal dusting takes place are not well identified as they have been reported to be 450-800°C [1, 2], 400-800°C [3], or 450-900°C [4, 5]. Conversely, in heat-treating industry, metal dusting has been reported to have occasionally occurred within the temperature range 900-930°C [6]. It has also been documented that metal dusting did happen at temperatures as high as 1100°C in heavily reducing environments [7]. In petrochemical plants, for example, metal dusting has been experienced in steam reforming furnaces used to manufacture synthesis gases (e.g. H_2, CO, and CO_2). The frequency of such failures has recently increased as plant operators tend to boost the process efficiency by introducing less steam to the system, thereby increasing the carbon monoxide content [8].

According to Grabke [9], metal dusting mechanism for nickel-based alloys involves the diffusion of carbon atoms through defects in the oxide layer into the alloy leading to formation of a carbon-supersaturated solution in the nickel matrix. Then, graphite deposits in different orientations on the alloy surface and starts to grow inward. The graphite growth is caused by carbon atoms from the solid solution attached to the graphite planes growing vertical to the alloy surface. This initiates

a localized degradation of the alloy and, as a result, metallic particles are released and transfer into the coke layer [10, 11]. Several modifications to this mechanism have also been suggested. For example, Pippel *et al.* [12] has proposed a mechanism which involves metal dissolution and diffusion into the graphite. The mechanism has been further discussed by Chun et al. [13]. Different mechanism has also been proposed by Zeng *et al.* [14] where carbon is thought to dissolve and diffuse to precipitate and accumulate at defects causing the nickel particles to separate. The surrounding gas, in turn, penetrates the cracked areas and deposits carbon leading to more metal dusting. The carbon continues to precipitate under the nickel and becomes a carbon filament.

In short, it is obvious that there is a still no universal agreement on metal dusting mechanisms as they are not fully understood although they have been studied for more than fifty years. Further research is needed to gain a better understanding of the mechanisms, particularly in high alloy metals [4, 12].

The objective of this study was to investigate the behaviour of three centrifugal casting, heat-resistant superalloys, namely KHR35C HiSi© (Alloy 1), KHR45A LC© (Alloy 2), and UCX© (Alloy 3), in metal dusting conditions. The alloys were exposed to a gas mixture containing 80 vol% CO+20 vol% H_2 and flowing at $100cm^3$ min^{-1} at 650, 750, and 850ºC for 100h. The chemical composition of the alloys is shown in Table-1.

Table-1. Chemical composition of the heat resistant alloys (wt. %).

	C	Fe	Cr	Ni	Si	Mn	Nb	W	Others
Alloy 1	0.45	35.9	25.1	35.1	1.6	0.9	0.9	---	Add.
Alloy 2	0.12	17.5	33.2	45.5	1.2	1.5	1.0	---	Add.
Alloy 3	0.28	5.0	40.4	50.2	2.2	0.8	---	1.1	Add.

ARPN Journal of Engineering and Applied Sciences

www.arpnjournals.com

Alloy 1 has an austenitic microstructure with chromium and niobium carbides outlining the boundaries. The microstructure of alloy 2 is also austenitic with a much lower concentration of primary carbides due to the alloy's lower carbon content. Alloy 3 also has an austenitic microstructure enriched with a network of interdendritic chromium carbides in addition to Zr/Ti nitrides [15].

MATERIALS AND METHODS

Alloy specimens were cut with dimension 20×20×5mm and ground to 120grit and their edges were rounded. The specimens were thoroughly washed in water and ultrasonically cleaned by acetone. A ceramic furnace tube, 1200mm long and 75mm ID, was used. The samples (one from each alloy) were suspended from an alumina rack by platinum wires and placed at the hot zone in the middle of the furnace. Cylinders of premixed 80 vol% $CO+20$ vol% H_2 were used to provide the experimental environment.

Before turning the furnace on, argon was introduced at $100cm^3 min^{-1}$ for one hour and then the gas mixture was switched on at $100cm^3 min^{-1}$ for one hour in order to establish the corrosion environment. On completion of the test, the samples were allowed to cool down in the gas mixture until the temperature reached 200°C where the system was purged with argon for one hour, and finally left to cool down to room temperature. Deposits on samples, if any, were mechanically removed by bristle brush and collected in containers for chemical analyses (SEM/EDX and XRD). The samples were thoroughly washed in water and ultrasonically cleaned in acetone. The alloys were analysed by XRD to identify phases present on their surfaces. The extent of corrosion was then assessed by scanning the sample surfaces firstly by optical microscope and secondly by SEM. Surface deposits and pit contents were chemically analyzed by EDX. The samples were cut in cross sections for further metallographic examination (SEM/EDX).

RESULTS AND DISCUSSIONS

Alloy 1

AT 650ºC

Exposing the alloy at 650ºC resulted in a considerable carbon deposition that almost covered the sample surface (Figure-1). Much growth of carbon filaments, especially on the sample sides, was also observed. Analyzing the deposit removed from this sample revealed the presence carbon as the main element. Traces of chromium and iron, and relatively high nickel and oxygen levels were also detected. SEM examination of the alloy surface revealed the development of a dense layer that was subsequently confirmed to be composed mainly of carbon, oxygen, silicon, chromium, iron, nickel, and some manganese (A1 in Figure-2). Some localized, darker deposits were also observed and found to contain major amounts of carbon, oxygen, in addition to traces of iron, chromium, and nickel (A2). The layer was found flaked

off in some areas, possibly by the cleaning process, allowing further examination of the surface underneath. Tiny pits, with a maximum size of about 1µm, could be seen spreading across the substrate. EDX of the pit contents showed the presence of higher levels of carbon compared to the surrounding areas. Randomly distributed pits, with different sizes and shapes, were observed across the alloy's cross section (Figure-3). The depth of the pits varied from approximately 20µm to 40µm. It was also noticed that some of the pits had linked up forming bigger perforation. The pits appeared to have initiated at the matrix rather than the carbides. Some pits were also observed to contain some alloy particles surrounded with carbon (Figure-4). Very wide pits (~55µm wide and ~21µm deep) were also seen on the alloy (Figure-5). In this Figure, it is interesting to observe that the attack tended to be more favourable through the bulk material rather than the carbides. The attack appeared to firstly grow vertically till it reached the grain boundary, where most of the primary carbides precipitated, and then turned to grow laterally through the matrix. Figure-6 shows higher magnification photomicrographs of the reaction front. A layer of fibrous and filament-like product had formed at the alloy substrate. Moreover, some carburisation was observed at the reaction zone. Analysis of the reaction front detected a mixture of alloying elements and carbon. The concentration of carbon within the layer was more in the inner part while more alloying elements, particularly chromium, were found at the outer layer. It is also worth noting that there was almost no oxygen at that layer suggesting a little formation of oxides.

AT 750ºC

No significant carbon filament growth was observed on the alloy after exposure at 750ºC and the degree of carbon deposition appeared to be considerably less than that took place at the 650ºC. However, comparatively dense carbon layers could be noticed on the sides of the sample. The analysis of the deposits found on this sample revealed the presence of mainly carbon and oxygen in addition to traces of nickel and iron. Figure-7 shows an image of the alloy surface revealing the presence of some localized metal removal. A layer of approximately 1µm typical thickness had grown on the alloy and was confirmed to contain oxides of mainly silicon, chromium, manganese, in addition to some iron and nickel. Interestingly, some darker phases were also observed embedded within that layer and contained significantly higher levels of carbon. Shallow, localized corrosion took place on the alloy and chunks of the base metal could be observed detached at some pits (Figure-8). EDX of the alloy substrate showed no significant reduction in the chromium level, which would have been expected to be consumed to produce oxides. However, there was no manganese detected in this area. Bands of carbides, precipitating in different directions, could be observed at the reaction zone, just beneath the pit. The product formed in the pit was composed of carbon and an oxides mixture in addition to possible free elements. The alloy chunk did

not contain any manganese (or niobium) suggesting that they were consumed during the oxidation process. It seemed that the scale built up and accumulated around the alloy portion eventually leading to disintegration. Figure-9 shows an alloy chunk that was not completely separated from the specimen. It seems that the attack was probably facilitated by the precipitation of some carbide bands and that created internal stresses and increased the substrate brittleness leading to carbon diffusion and oxidation assisted crack propagation.

AT 850ºC

The alloy experienced extremely low carbon deposition following the exposure at 850ºC. Instead, the surface of the alloy was mainly covered with a grey layer. The layer was confirmed to contain very high levels chromium-manganese oxide were in addition to iron and nickel as minor elements. A cross section of the alloy is shown in Figure-10. No significant metal removal was noticed except the presence of some shallow pits. However, very distinctive strips of carbides appeared to have formed at the reaction zone. Moreover, the alloy was covered with what appeared to be a non homogeneous layer. Elemental analysis of the substrate did not show significant depletion of the oxide-forming elements. An internal layer (P3), of about 1µm, was observed at the alloy substrate and EDX confirmed this to be a chromium-based oxide. An external darker, thicker, layer that contained more silicon oxides and carbon had formed above the oxide scale. Some chromium, manganese, and silicon oxide particles were also observed embedded within the layer formed at the pit (P1).

Alloy 2

AT 650ºC

Apart from a few carbon filaments seen on the sides, this alloy did not experience an appreciable carbon deposition. Analysis of the deposit removed from this sample showed that it was composed mainly of carbon and oxygen with traces of chromium and nickel. Indeed, the presence of alloying elements such as chromium, nickel, and/or iron in the deposit might well suggest the onset of metal dusting. The alloy surface had been covered with a layer that was found to contain mainly chromium and oxygen suggesting the development of Cr_2O_3. Also, large amounts of silicon, nickel, and manganese were detected. Examination of the alloy surface also revealed the presence of small pits with a maximum size of approximately 2.5µm. A few pits were observed along the sample cross section. Figures 11 and 12 summarise a detailed investigation carried out on one of the pits that was ~9µm deep. The pit appeared to grow in different directions within the alloy. The deposits and layers inside the pit were analyzed (A1, A2, A3 and A4) and found to contain mixtures of carbon and oxides. Examination of the micrograph showed that the substrate suffered carburisation as a high concentration of carbides was noticed surrounding the pit. A thin layer, approximately

0.5µm, was also observed to have formed on the alloy and found to be composed of carbon and oxides (A8).

AT 750ºC

A little carbon deposition had taken place on the alloy and the deposit removed from this specimen was composed of carbon as main constituent and oxygen in addition to traces of iron and nickel. There appeared to be two layers formed on the alloy; the outer contained a mixture of carbon and oxygen and traces of alloying element whilst the inner contained oxides of chromium, silicon, and manganese with a much lower amount of carbon. Localized attack, approximately 7µm deep, was also observed on this sample (Figure-13). It seemed that the attack stopped growing after sometime as the reaction front appeared to be smooth and covered with a continuous layer. No significant reduction in scale-forming elements, particularly chromium, was detected at the substrate meaning that only mild oxidation might have taken place at the pit bottom. Spherical chromium carbides were also observed at the reaction zone. Different areas on the layer, which was approximately 1.2µm thick, were analyzed and found to have different composition. For example, an area (A1) was found to have high level of carbon (37.7 wt %) whereas only a minor amount (2 wt %) was found at another area (A2) and the same applied for chromium.

AT 850ºC

The alloy experienced almost no carbon deposition and instead, the surface was covered mainly with a light greenish layer. As seen in Figures 14 and 15, the alloy experienced pitting of approximately 8µm maximum depth and the pits were randomly distributed across the specimen cross section. A close up examination of the pits revealed the presence of different layers on the alloy surface. Internal islands of oxides (A4 in Figure-15) were noticed to grow into the reaction zone at the bottom of the pits. These islands contained large amounts of chromium and manganese oxides. The layer formed in the pit bottom (A3) was also found to contain chromium and manganese oxides. Higher carbon levels were detected at the darker areas (A1 and A2). The area, A5, located between two oxide islands, was analyzed and found to contain high concentration of chromium. Figure-16 shows a high magnification micrograph of the alloy substrate (not a pitting site) where two phases could be clearly seen. The layer, which was in total ~2.3µm thick, was analyzed to identify the composition of the two phases. The darker, outer layer (A1) was composed mainly of carbon and silicon oxides. The inner layer (A2), however, comprised chromium, manganese, and silicon oxides with comparatively lower amount of carbon.

Alloy 3

AT 650ºC

Visual inspection of the alloy revealed extremely low carbon deposition. The surface was however entirely

www.arpnjournals.com

covered with a layer that was found to be composed of oxides of chromium, silicon, and manganese. Considerable amounts of nickel (11.9 wt %) and iron (1.8 wt %) were also detected. Some deposit islands that seemed to be residuals from an external layer, which was possibly removed by cleaning, were also analyzed and found to have carbon as the main constituent with comparatively low oxygen levels. Examining the cross section of the sample showed that the alloy did not experience significant metal dusting. However, a few isolated, shallow pits still could be observed (Figure-17).

AT 750ºC

Mild carbon deposition was observed on the sample. The exposure however resulted in formation of an approximately 5µm, uneven chromium oxide-rich layer (Figure-18). Carbon at low levels was also detected at the scale. No significant pitting was noticed on the alloy or along the cross section. EDX of the layer indicated increasing carbon levels in the outer part of the layer. Also, high amount of nickel and iron was detected at the layer. The oxides formed were mainly those of chromium and silicon.

AT 850ºC

A grey layer, which had been lighter in some places, was visually observed to have formed on the sample. Superficial pitting appeared to have occurred on the alloy surface (Figure-19). A close up image of one of the pits is shown in Figure-20. Considerable amounts of silicon, chromium, and nickel were detected within the carbon deposit at the pit. Also, the particles embedded inside the pit (indicated by the arrow in Figure-20) were found to contain high levels of chromium, iron, and nickel.

CONCLUSIONS

a) Increasing the exposure temperature generally caused less carbon deposition and more oxides formation on the alloys leading to a reduction in the attack aggressiveness.

b) Deposits collected from the samples and contained metal, oxides, and probably carbide particles which indicated the onset of metal dusting.

c) Alloy 1 suffered metal dusting in form of pitting at 650ºC. The pits initiated at the matrix rather than the primary carbides and also progressed through the matrix. The attack process involved inward diffusion of carbon followed by growth of very small filaments into the reaction front which induced internal stress at the substrate and caused alloy disintegration.

d) Alloy 1 also experienced pitting after 750ºC but the attack was less aggressive than that observed at 650ºC. Isolated alloy particles were seen at the pits after 100h and layers of carbon and oxides accumulated around them. Although these particles might have been removed during sample preparation, it seemed that the attack was probably facilitated by the precipitation of some carbide bands and that created internal stresses that caused microcracking

leading to carbon diffusion and oxidation-assisted crack propagation.

e) The least attack observed on Alloy 1 was after the exposure at 850ºC. The least attack accompanied with little carbon deposition and most oxides formation was observed on the alloy as a result of exposure at 850ºC. The alloy reaction zone suffered carburisation after 100h and some of the carbides precipitated in form of relatively long bands.

f) Pitting occurred on Alloy 2 after 650ºC but to a less extent compared with HP. A few pits were observed along the sample cross section and they appeared to grow in different directions within the alloy.

g) A few pits were observed on Alloy 2 exposed at 750ºC. The mechanism by which the attack took place was similar to that observed on the alloy at 650ºC. However, more oxides formed on the alloy as a result of increasing the temperature to 750ºC.

h) The least pitting on Alloy 2 was observed after 850ºC. Slightly different pitting was seen after exposure at 850ºC where, in addition to the oxide layer formed at the pit's bottom, internal islands of oxides grew into the substrate.

i) Although it did not show a complete immunity, Alloy 3 proved to be the most resistant alloy to metal dusting at the test temperatures.

ACKNOWLEDGEMENTS

REFERENCES

[1] Jones Richard T, Kenneth L. Baumert. 2001. Metal Dusting-An Overview of Current Literature. NACE International Corrosion. Paper No. 01372.

[2] E. Pippel, J. Woltersdrof and R. Schneider. 1998. Micromechanisms of Metal Dusting on Fe-Base and Ni-Base alloys. Materials and Corrosion. 49: 309-316.

[3] Baker Brian A. and Gaylord D. Smith. Metal Dusting Behaviour of High Temperature Alloys. NACE International Corrosion. 99, Paper No. 54.

[4] Agarwal D.C., U. Brill and Jutta Kloewer. 2001. Recent Results on Metal Dusting of Nickel Base Alloys and Some Applications. NACE International Corrosion, Houston.

[5] Lai George Y. 1997. High-Temperature Corrosion of Engineering Alloys. ASM International, USA.

[6] Kelly James, Jason Wilson and Devin Wachowiak. 2004. Metal Dusting a.k.a Carbon Rot in the Heat Treat Industry, 50 years, July. www.rolledalloys.com.

www.arpnjournals.com

[7] Hrivnak Ivan, Lubomir Caplovic, Gejza Bakay and Aurel Bitter. 2005. Metal Dusting of Inlet Tube Made of Alloy 800. Kovove Mater. 43: 290-299.

[8] Di Gabriele F., J. R. Bernstein, M. M. Al-Qhatani, Z. Liu, M. P. Jordan, J. A. Richardson and F. H. Stott. 2003. Study of the Metal Dusting Behaviour of High Temperature Alloys. Materials and Corrosion. 54(11).

[9] Grabke H. J. 2003. Metal Dusting. Materials and Corrosion. 54(10).

[10] Kirchheiner R. and J. L. Jimenez Solar. 2001. Correlation of Oxidation, Carburisation and Metal Dusting- Controlling Corrosion by Corrosion. NACE International Corrosion. Paper No. 01374.

[11] Pippel E., J. Woltersdorf and H. J. Grabke. 2003. Microprocesses of Metal Dusting on Iron-Nickel Alloys and Their Dependence on Composition. Materials and Corrosion. 54(10): 747-751.

[12] Szakalos Peter. 2004. Mechanisms of Metal Dusting. PhD Thesis. Department of Material Science and Engineering, Division of Corrosion Science, Royal Institute of Technology, Sweden and Swedish Institute for Metals Research, Sweden.

[13] Chun C. M., J. D. Mumford and T. A. Ramanarayanan. 2000. Carbon Induced Corrosion of Nickel Anode. Journal of Electrochemical Society. 147(10): 3680-3686.

[14] Zeng Z. and K. Natesan. 2005. Relationship between the Growth of Carbon Nanofilaments and Metal Dusting Corrosion. Chem. Mater. 17: 3794-3801.

[15] Al-Meshari Abdulaziz and John Little. 2008. Oxidation of Heat-Resistant Alloys. Oxidation of Metals. 69: 109-118.

ARPN Journal of Engineering and Applied Sciences

www.arpnjournals.com

CAPTIONS

Figure-1. General photo of the alloys after exposures at 650ºC.

Figure-2. Alloy 1 suffered pitting attack after exposure at 650ºC.

Figure-3. Relatively wide pits observed on Alloy 1 after exposure at 650ºC.

Figure-4. Pits contained alloy particles surrounded with carbon seen on Alloy 1 after exposure at 650ºC.

Figure-5. Wide pits found on Alloy 1 surface after exposure at 650ºC.

Figure-6. A layer of fibrous and filament-like product had formed at the reaction front of pit shown in Figure-5.

Figure-7. Localized attack observed Alloy 1 substrate after exposure at 750ºC.

Figure-8. Localized corrosion took place on Alloy 1 and detached chunks of the base metal observed after exposure at 750ºC.

Figure-9. A micrograph showing the progress of metal removal process on Alloy 1 after exposure at 750ºC.

Figure-10. Presence of some shallow pits on Alloy 1 after exposure at 850ºC.

Figure-11. Localized attack took place on Alloy 2 after exposure at 650ºC.

Figure-12. Further analysis to the layers formed within the attack area shown first in

Figure-13. Localized corrosion seen on Alloy 2 after 100h at 750ºC.

Figure-14. Pits formed on Alloy 2 after exposure at 850ºC.

Figure-15. EDX of a pit on Alloy 2 caused by exposure at 850ºC.

Figure-16. Layer formed on Alloy 2 surface after 100h at 850ºC.

Figure-17. Cross section of Alloy 3after 100h at 650ºC.

Figure-18. Cross section of Alloy 3 after exposure at 750ºC for 100h.

Figure-19. Cross section of Alloy 3 after exposure at 850ºC for 100h.

Figure-20. A higher magnification image of a pit formed on Alloy 3 after 100h at 850ºC.

Figure-1.
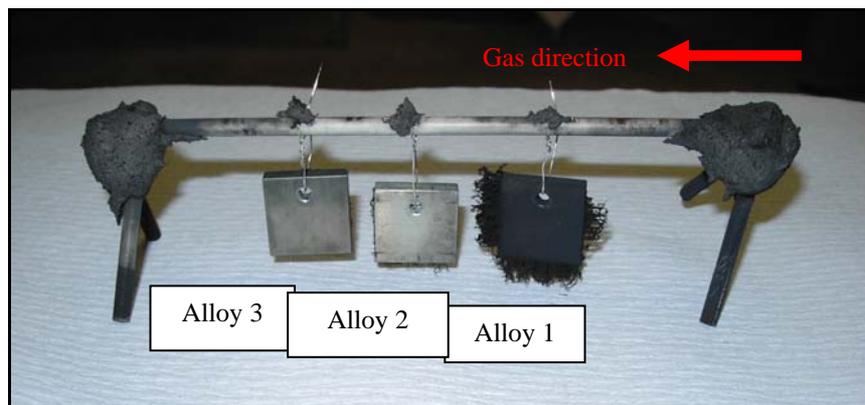
www.arpnjournals.com
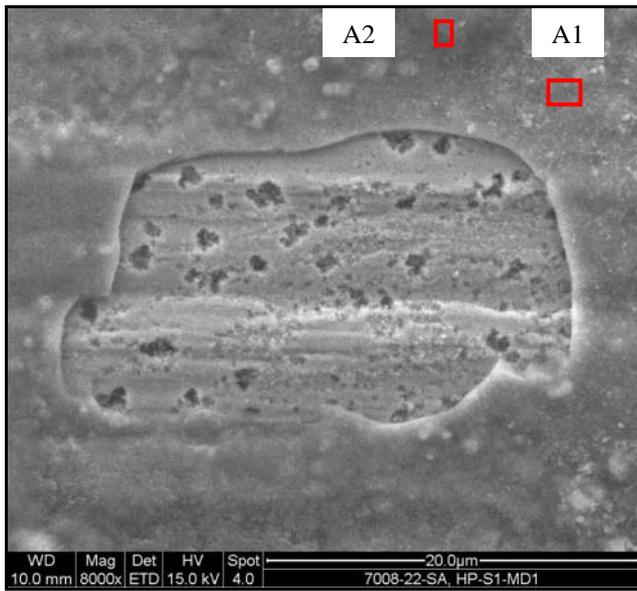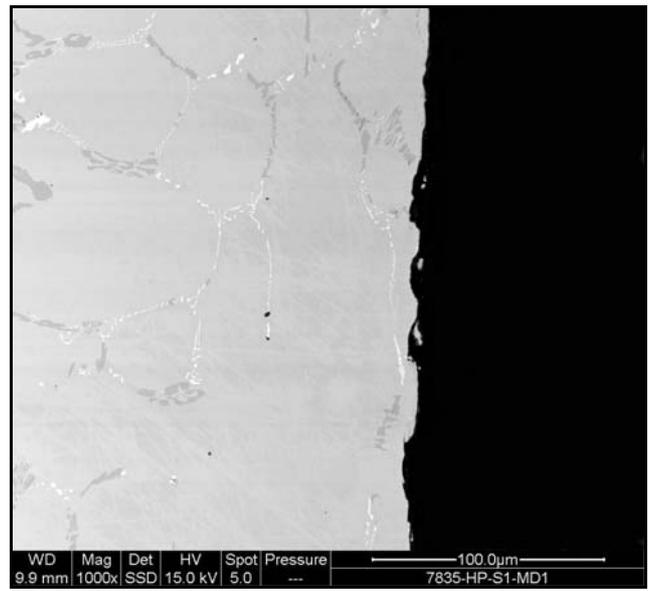
Figure-2.

Figure-4.

Figure-3.
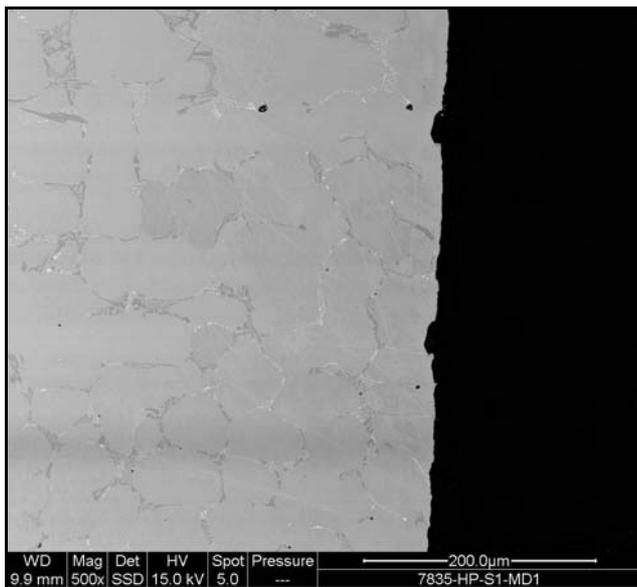
Figure-5.
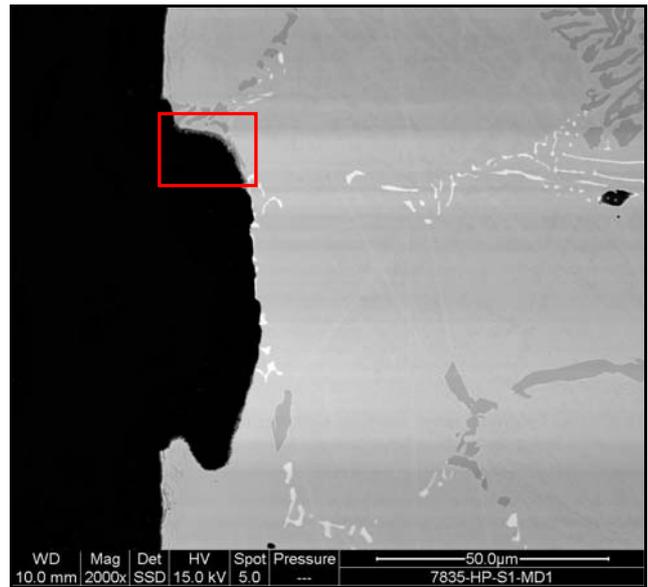
www.arpnjournals.com
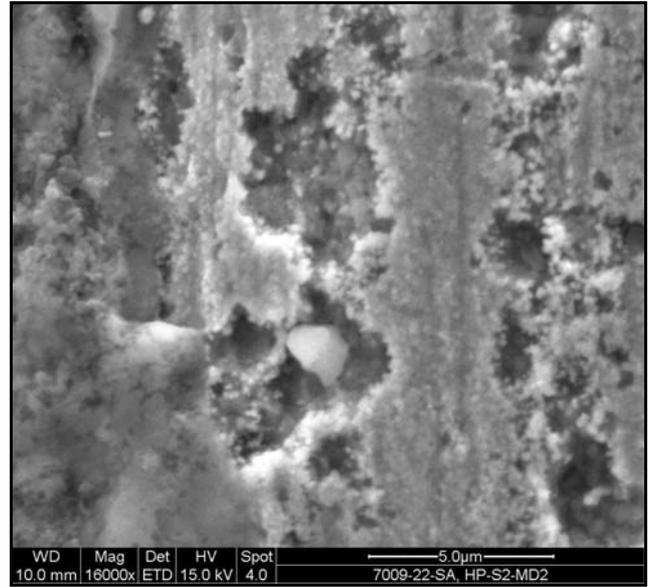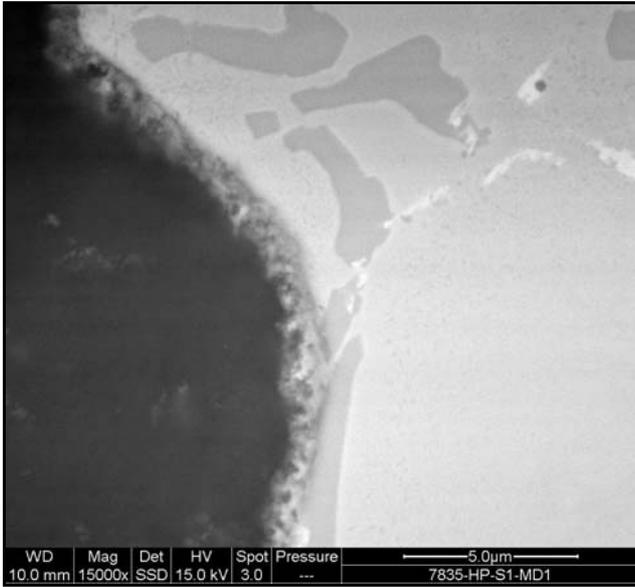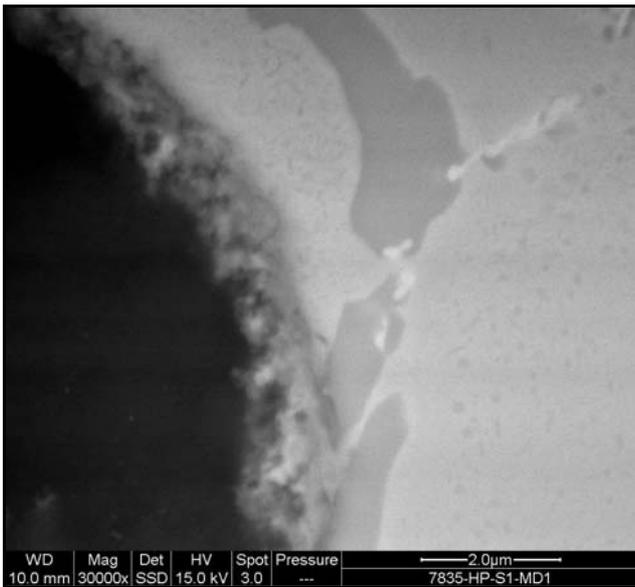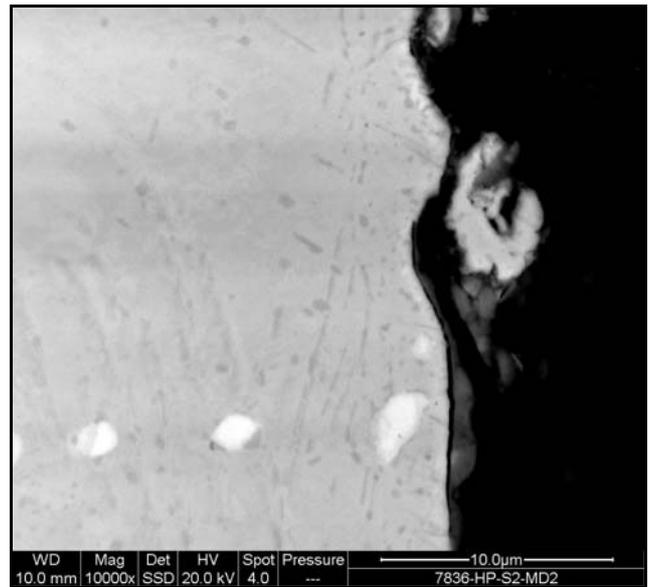
Figure-7.

Figure-6.

Figure-8.

www.arpnjournals.com
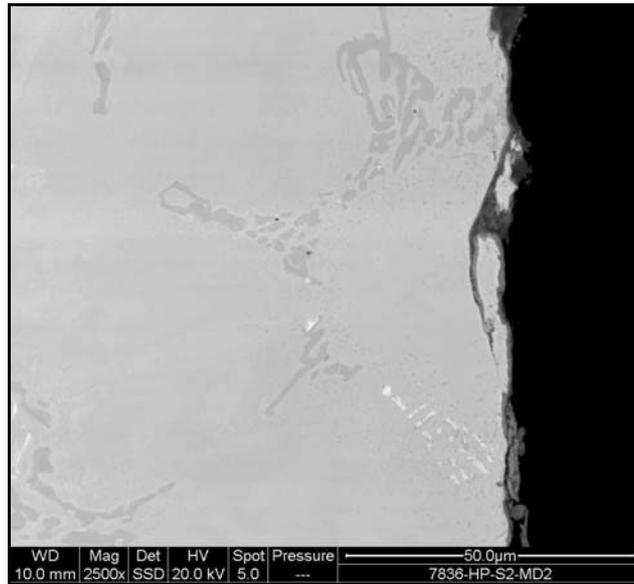
Figure-9.
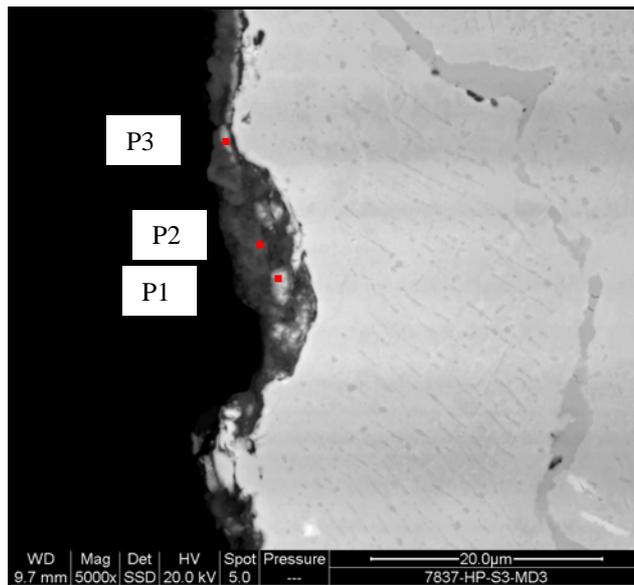
	P1			**P2**			**P3**	
Element	**Wt%**	**At%**	**Element**	**Wt%**	**At%**	**Element**	**Wt%**	**At%**
C K	12.71	25.37	C K	28.69	38.48	C K	17.70	31.09
O K	29.60	44.36	O K	48.14	48.48	O K	36.09	47.59
Si K	10.06	8.59	F K	1.04	0.88	Si K	8.27	6.21
Ca K	0.32	0.19	Mg K	0.22	0.15	Ca K	0.47	0.25
Cr K	35.52	16.38	Si K	19.75	11.33	Cr K	24.20	9.82
Mn K	8.48	3.70	Ca K	0.40	0.16	Mn K	9.27	3.56
Fe K	2.40	1.03	Cr K	0.69	0.21	Fe K	2.33	0.88
Ni K	0.90	0.37	Mn K	0.33	0.10	Ni K	1.67	0.60
			Fe K	0.43	0.13			
			Ni K	0.32	0.09			
Total	**100.00**		**Total**	**100.00**		**Total**	**100.00**	

Figure-10.

www.arpnjournals.com
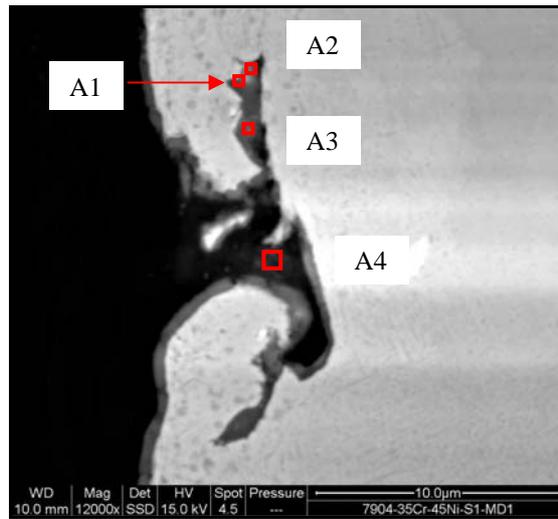
| | A1 | | | A2 | | | A3 | | | A4 | |
	Wt%	**At%**		**Wt%**	**At%**		**Wt%**	**At%**		**Wt%**	**At%**
C K	1.45	3.70	C K	1.58	4.76	C K	9.76	25.24	C K	36.79	57.39
O K	26.15	50.17	O K	16.49	37.26	O K	15.06	29.25	O K	21.20	24.83
Si K	9.77	10.67	Si K	6.25	8.05	Si K	4.82	5.33	Si K	8.98	5.99
Ca K	0.26	0.20	Ca K	0.32	0.29	Ca K	0.45	0.35	S K	0.21	0.12
Cr K	31.70	18.71	Cr K	32.91	22.88	Cr K	32.99	19.71	Ca K	2.25	1.05
Mn K	8.92	4.98	Mn K	6.40	4.21	Mn K	9.93	5.62	Cr K	17.43	6.28
Fe K	7.33	4.03	Fe K	11.24	7.27	Fe K	7.95	4.42	Mn K	1.62	0.55
Ni K	14.43	7.54	Ni K	24.82	15.28	Ni K	19.05	10.08	Fe K	6.69	2.24
									Ni K	4.82	1.54
Total	**100.0**		**Total**	**100.0**		**Total**	**100.0**		**Total**	**100.0**	

Figure-11.

www.arpnjournals.com
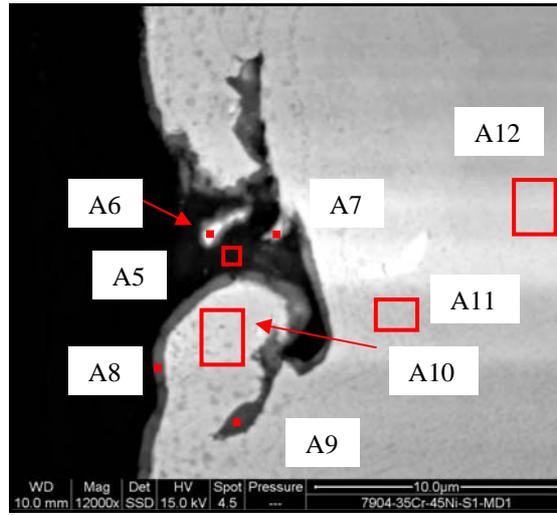
	A5			**A6**			**A7**			**A8**	
	Wt%	**At%**		**Wt%**	**At%**		**Wt%**	**At%**		**Wt%**	**At%**
C K	50.42	65.86	C K	48.87	66.50	C K	17.87	40.82	C K	4.27	15.13
O K	24.02	23.56	O K	21.28	21.73	O K	10.32	17.69	O K	5.55	14.74
Si K	11.46	6.40	Si K	10.01	5.83	Si K	6.80	6.64	Si K	2.22	3.37
Ca K	0.82	0.32	Ca K	0.36	0.15	Ca K	10.37	7.09	Ca K	0.27	0.29
Cr K	7.85	2.37	Cr K	8.63	2.71	Cr K	29.93	15.79	Cr K	24.63	20.15
Mn K	0.75	0.22	Mn K	0.60	0.18	Mn K	4.33	2.16	Fe K	17.40	13.25
Fe K	1.98	0.56	Fe K	3.32	0.97	Fe K	11.47	5.63	Ni K	45.66	33.08
Ni K	2.69	0.72	Ni K	6.92	1.93	Ni K	8.91	4.16			
Total	**100.0**		**Total**	**100.0**		**Total**	**100.0**		**Total**	**100.0**	

	A9			**A10**			**A11**			**A12**	
	Wt%	**At%**		**Wt%**	**At%**		**Wt%**	**At%**		**Wt%**	**At%**
C K	2.12	8.64	C K	7.78	20.32	C K	1.87	7.75	C K	1.60	6.68
O K	1.97	6.01	O K	17.92	35.15	O K	1.69	5.26	O K	1.72	5.40
Si K	1.42	2.47	Si K	5.22	5.83	Si K	1.30	2.30	Si K	1.33	2.38
Cr K	31.80	29.91	Ca K	0.28	0.22	Cr K	33.20	31.76	Cr K	32.98	31.78
Fe K	17.64	15.44	Cr K	25.24	15.23	Mn K	1.65	1.49	Mn K	1.41	1.29
Ni K	45.05	37.53	Mn K	3.33	1.90	Fe K	16.65	14.82	Fe K	16.79	15.06
			Fe K	10.78	6.05	Ni K	42.55	36.04	Ni K	43.31	36.96
			Ni K	27.21	14.54	Nb L	1.09	0.58	Nb L	0.85	0.46
			Nb L	2.24	0.76						
Total	**100.0**		**Total**	**100.0**		**Total**	**100.0**		**Total**	**100.0**	

Figure-12.

www.arpnjournals.com
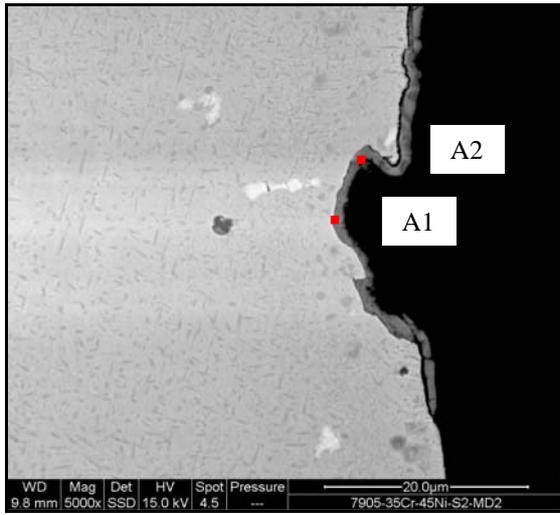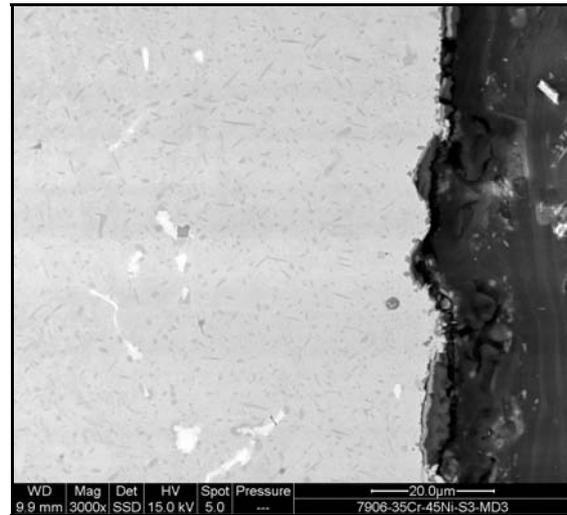
Figure-13.

Figure-14.
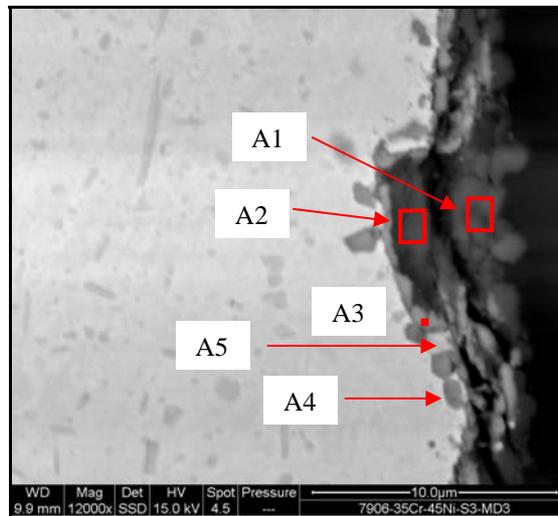
A1			A2			A3		
Element	**Wt%**	**At%**	**Element**	**Wt%**	**At%**	**Element**	**Wt%**	**At%**
C K	29.53	39.39	C K	4.12	6.49	C K	1.48	3.35
O K	47.79	47.85	O K	58.72	69.38	O K	36.15	61.47
Mg K	0.24	0.16	Si K	34.30	23.09	Si K	6.77	6.56
Si K	21.59	12.31	Ca K	0.16	0.07	Ca K	0.33	0.22
Ca K	0.38	0.15	Cr K	2.08	0.76	Cr K	37.82	19.79
Cr K	0.47	0.15	Mn K	0.62	0.21	Mn K	15.73	7.79
						Fe K	0.75	0.37
						Ni K	0.96	0.45
Total	**100.00**		**Total**	**100.00**		**Total**	**100.00**	

ARPN Journal of Engineering and Applied Sciences

www.arpnjournals.com

A4			A5		
Element	**Wt%**	**At%**	**Element**	**Wt%**	**At%**
C K	1.51	3.89	C K	1.45	4.61
O K	28.48	54.98	O K	13.86	33.12
Si K	1.47	1.62	Si K	0.95	1.29
Ca K	0.26	0.20	Ca K	0.39	0.37
Ti K	0.29	0.19	Cr K	70.90	52.12
Cr K	38.44	22.83	Mn K	4.77	3.32
Mn K	17.83	10.03	Fe K	5.27	3.61
Fe K	3.89	2.15	Ni K	2.42	1.57
Ni K	7.83	4.12			
			Total	**100.00**	
Total	**100.00**		C K	1.45	4.61

Figure-15.
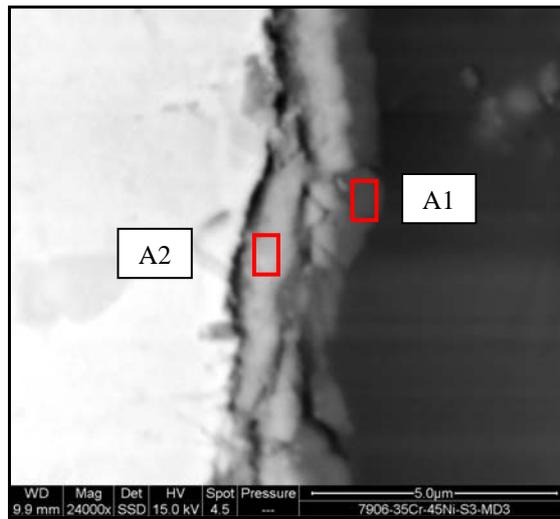
A1			A2		
Element	**Wt%**	**At%**	**Element**	**Wt%**	**At%**
C K	45.48	56.34	C K	8.15	15.69
O K	37.42	34.80	O K	39.57	57.21
F K	0.98	0.77	Si K	10.90	8.98
Na K	0.17	0.11	Ca K	0.33	0.19
Mg K	0.43	0.26	Cr K	28.64	12.74
Al K	0.12	0.07	Mn K	10.71	4.51
Si K	13.15	6.97	Fe K	0.74	0.31
Ca K	0.53	0.20	Ni K	0.96	0.38
Cr K	1.32	0.38			
Mn K	0.39	0.11			
Total	**100.00**		**Total**	**100.00**	

Figure-16.

www.arpnjournals.com
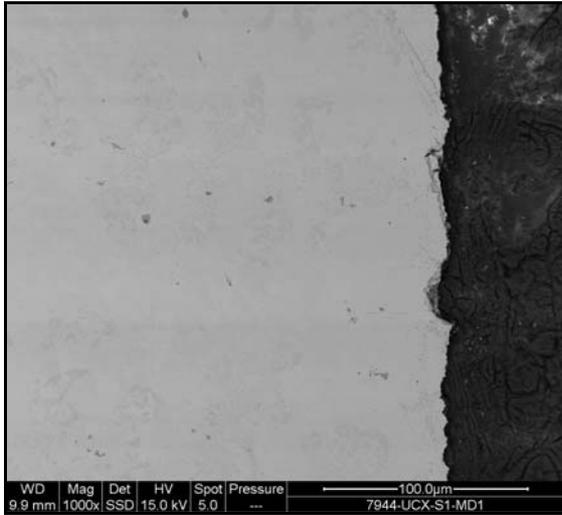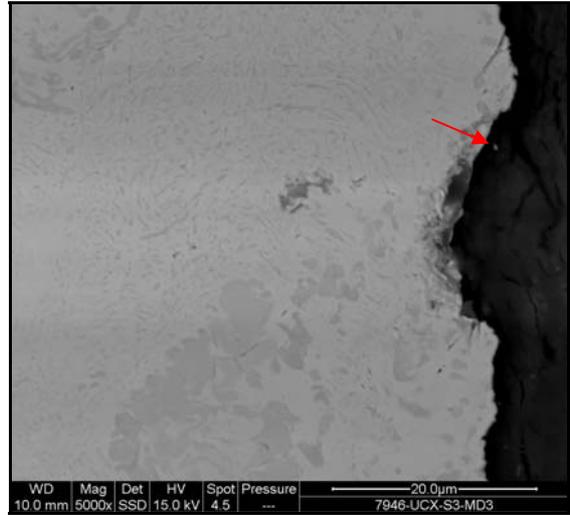
Figure-17.

Figure-20.

Figure-18.

Figure-19.